Long Non-coding RNA PANDAR Promotes Radioresistance in Nasopharyngeal Carcinoma via SIRT1/Ku70/PI3K/Akt Pathway

Si-wei Li
Huazhong Hospital
Guo-liang Pi
Hubei Cancer Hospital
Yong Zeng
Huanggang Central Hospital
Chang-li Ruan
Renmin Hospital of Wuhan University: Wuhan University Renmin Hospital
Xiao-song He
The Affiliated Hospital of Guilin Medical University
Xiao-xia Xiong
Huangzhou Hospital
Man Zhang
Huangzhou Hospital
Guang Han
Huangzhou Hospital
xinjun Liang (Liangxinjun2541@163.com)
Hubei Cancer Hospital https://orcid.org/0000-0002-5221-6589

Research article

Keywords: Nasopharyngeal carcinoma, Radioresistance, Long non-coding RNA promoter of CDKN1A antisense DNA damage activated RNA, Sirtuin 1, Ku70, PI3K/Akt pathway

Posted Date: September 30th, 2021

DOI: https://doi.org/10.21203/rs.3.rs-762963/v1

Abstract

Objective: Radioresistance may result in nasopharyngeal carcinoma (NPC) radiation failure. To comprehend the concrete mechanism in NPC radioresistance, this work was initiated from long non-coding RNA (lncRNA) promoter of CDKN1A antisense DNA damage activated RNA (PANDAR), accompanied by sirtuin 1 (SIRT1), Ku70, and phosphatidylinositol 3 kinase (PI3K)/Akt pathway.

Methods: NPC cancer tissues and normal tissues were harvested and NPC cancer tissues were specified into radioresistant and radiosensitive types. The connection between PANDA expression with NPC radioresistance, clinicopathological traits and prognosis was tested. Radioresistant CNE2-IR and 5-8F-IR cells were induced and transfected with depleted PANDAR or SIRT1 to identify their roles in cell proliferation, cycle distribution, apoptosis, SIRT1, Ku70 and PI3K/Akt pathway. PANDA and SIRT1 expression in CNE2-IR and 5-8F-IR cells were tested.

Results: PANDA was elevated in NPC tissues and radioresistant tissues relative to normal tissues and radiosensitive tissues. Raised PANDA was connected with NPC radioresistance and unsatisfactory prognosis. CNE2-IR and 5-8F-IR cells expressed up-regulated PANDA and SIRT1. Down-regulating PANDA or SIRT1 inhibited radioresistant NPC cell proliferation, decreased SIRT1 and Ku70, and inactivated PI3K/Akt pathway.

Conclusion: This work has clued that depleting PANDA decreases SIRT1 recruitment to inactivate Ku70 deacetylation-mediated PI3K/Akt pathway, thereby promoting NPC radiosensitivity.

Introduction

Nasopharyngeal carcinoma (NPC) belongs to the category of head and neck malignancy, which is featured by unsatisfactory prognosis and high recurrence [1]. The prevailing treatment for NPC is radiotherapy combined with or without concurrent chemotherapy, of which the efficacy is partially restricted to intrinsic and acquired radioresistance [2]. In a reviewed analysis, cancer stem cells, abnormal activation of certain signaling pathways, mutation and epigenetic modification of genes, formation of stress granules and changes of tumor microenvironment are attributable to NPC radioresistance [3]. Owing to the radioresistance in the treatment of NPC, improving NPC radiosensitivity is a quite urgent demand.

The applicable potency of long non-coding RNAs (lncRNAs) in NPC radioresistance has been delved in a wide range. Actually, lncRNA MYC-induced long non-coding RNA (MINCR) is reported to affect radiotherapy efficacy of NPC, as reflected by MINCR overexpression impairing NPC cell radiosensitivity [4]. Moreover, lncRNA plasmacytoma variant translocation 1 depletion is weaponed to improve NPC radiosensitivity by hindering cell proliferation and enhancing apoptosis rate [5]. Supportively, it is witnessed that down-regulated lncRNA Antisense Noncoding RNA in the INK4 Locus suppresses proliferation and induces apoptosis, thereby to enable NPC cells to be radiosensitive [6]. As to lncRNA promoter of CDKN1A antisense DNA damage activated RNA (PANDAR), studies have identified it as an

up-regulated oncogenic gene in cancers, such as breast cancer, colorectal cancer and gastric cancer [7–9]. However, the mechanism of PANDAR in NPC progression and radioresistance has been seldom elucidated. Sirtuin 1 (SIRT1) regulation has been implied to control NPC cell growth and apoptosis [10]. Promisingly, it is developed that taking control of SIRT1-related pathway may be crucial for protecting against tumorigenesis [11]. Mechanistically, SIRT1 can mediate target genes via deacetylation, such as Ku70 [12], a DNA damage/repair protein which is positioned in X-ray irradiation in NPC treatment [13]. Moreover, transcriptional inhibition of Ku70/80 obstructs NPC cell progression and enhances NPC cell radiosensitivity [14]. Phosphatidylinositol 3 kinase (PI3K)/AKT pathway activation has once been discussed to facilitate proliferation and repress apoptosis of NPC cells [15]. Also, by inhibiting PI3K/AKT pathway activation, NPC tumor expansive and metastatic behaviors are destroyed [16]. Consulted from the existed studies, it is observed that the combination of PANDAR, SIRT1, Ku70 and PI3K/AKT pathway is not thoroughly elaborated in NPC radioresistance, which is the original enlightenment for initiating this study.

Materials And Methods

Ethics statement

This study was reviewed and approved by the ethics committee of Hubei Cancer Hospital, Tongji Medical College, Huazhong University of Science and Technology. All patients have signed an informed consent.

Experimental subjects

NPC patients (n = 89) who underwent radiotherapy in Hubei Cancer Hospital, Tongji Medical College, Huazhong University of Science and Technology from July 2012 to July 2014 were included. All cases (51 males and 38 females) were diagnosed by pathological examination and had complete clinical data. According to tumor node metastasis (TNM) stage in the Chinese 2008 staging system for NPC [17], 11 cases were in stage Ⅰ, 36 cases in stage Ⅱ, 23 cases in stage Ⅲ and 28 cases in stage Ⅳ; 19 cases with cervical lymph node metastasis (LNM) and the other 61 cases without. In terms of N stage, 27 cases were in N0, 11 cases in N1, 44 cases in N2, and 7 cases in N3. There were 40 cases of squamous cell carcinoma, 33 cases of non-keratinizing carcinoma and 26 cases of undifferentiated carcinoma. None NPC patients had received anti-cancer treatment such as radiotherapy or chemotherapy before biopsy. Cancer tissue and 40 normal nasopharyngeal mucosa tissue specimens were fixed in formalin and embedded in paraffin. Normalized by the criteria [18], NPC patients were categorized into radioresistance (n = 42) and radiosensitivity (n = 47). Postoperative follow-up (60 months, end at July 30, 2019) was programmed by outpatient clinics or telephone calls.

Cell selection and culture

Human NPC cells 6-10B, CNE2, 5-8F, HONE1 and C666-1 (Sun Yat-sen University, Guangzhou, China; Xiangya Medical College of Central South University, Changsha, China), human normal nasopharyngeal epithelial cell line NP69 (Shanghai Jianglin Biotechnology Technology Co., Ltd., Shanghai, China) were

cultured in Roswell Park Memorial Institute 1640 medium (Gibco, Grand Island, NY, USA) supplemented with 10% fetal bovine serum (Gibco). With the medium renewed every 2 days, cells were cultured into 80% confluence and detected by reverse transcription quantitative polymerase chain reaction (RT-qPCR).

Radioresistant CNE2-IR and 5-8F-IR cell induction

CNE2 and 5-8F cells (1× 10^5 cells) were seeded in T25 flask with Dulbecco's modified Eagle medium (Invitrogen, Carlsbad, CA, USA) with 10 % fast calcification solution (Invitrogen) and 1 % antibiotics. Treated with 4 rounds of sublethal ionizing radiation (13 Gy), CNE2 and 5-8F cells were induced to be radioresistant [19]. Then, the survived CNE2 and 5-8F cells were subcultured into passage 1, which were then treated with a sublethal dose of irradiation. Next, the survived CNE2 and 5-8F cells were subcultured to passage 4, which were named as CNE2-IR and 5-8F-IR. CNE2 and 5-8F cells, regarded as a control, were treated with the same procedure, except they were sham irradiated. CNE2-IR and 5-8F-IR cells in 4–10 passages after irradiation termination were utilized for experiments.

Cell transfection

Pre-seeded into 24-well cell culture plates at 1 × 10^5 cells/mL, CNE2-IR and 5-8F-IR cells (1 mL) were cultured to 80% confluence and transfected with sequences (GenePharma, Shanghai, China) in compliance with the instructions of lipofectamine 2000 (Invitrogen).

CNE2-IR and 5-8F-IR cells were transfected with PANDAR low expression vector negative control (NC), PANDAR low expression vector, SIRT1 low expression vector NC, SIRT1 low expression vector, or PANDAR low vector and SIRT1 overexpression vector.

Parental CNE2 and 5-8F cells were transfected with PANDAR overexpression vector NC, PANDAR overexpression vector, SIRT1 overexpression vector NC, SIRT1 overexpression vector, or PANDAR overexpression vector and SIRT1 low expression vector.

Colony formation assay

After exposure to radiation, NPC radioresistance was measured by colony formation assay. CNE2-IR and 5-8F-IR cells of passage 4 and parental CNE-2 and 5-8F cells were seeded in 6-well culture plates and exposed to radiation (2–10 Gy). Then, the cells were cultured for 12 d to record survived colony number (a colony > 50 cells). Cell survival fraction was calculated as (the number of colonies/the number of seeded cells) × seeding efficiency. Seeding efficiency was calculated as colonies per 10 cells.

Cell counting kit-8 (CCK-8) assay

CNE2-IR and 5-8F-IR cells were cultured in 96-well plates at 1 × 10^4 cells/well for 12 h and irradiated at 6 Gy. Then, cell proliferation was observed within 72 h. CCK-8 reagent (10 μL, Beyotime, Shanghai, China) was added into cells per well and detected on a microplate reader (Thermo Fisher Scientific, MA, USA) at 450 nm/630 nm. Cell proliferation curve was drawn with irradiation dose as the abscissa and optical density (OD) value as the ordinate.

Flow cytometry

CNE2-IR and 5-8F-IR cells were cultured on a 6-well culture plate for 12 h and irradiated at 6 Gy. Subsequently, the cells were cultured for 48 h, following trypsinization and centrifugation. The cell pellet was soaked with cold PBS and centrifuged once again. In conformity with the instructions of Annexin-V-fluorescein isothiocyanate (FITC) Apoptosis Detection Kit (Beyotime), Annexin-V-FITC, PI and HEPES buffer (1:2:50) were prepared into Annexin-V-FITC/PI solution, in which cells (1×10^6 cells per 100 μL staining solution) were incubated for 15 min and HEPES buffer (1 mL) was added. Cell apoptosis was tested by FITC and PI fluorescence (488 nm excitation wavelength to excite 525 nm and 620 nm band-pass filters). With AnnexinV as the horizontal axis and PI as the vertical axis, the upper left quadrant $(AnnexinV\text{-}FITC)^-/PI^+$ stood for necrotic cells, containing some late apoptotic and mechanically damaged cells, upper right quadrant $(AnnexinV + FITC)^+/PI^+$ for late apoptotic cells, lower right quadrant $(AnnexinV\text{-}FITC)^+/PI^-$ for early apoptotic cells and lower left quadrant $(AnnexinV\text{-}FITC)^-/PI^-$ for living cells. Apoptosis rate (%) = (early apoptotic cells + late apoptotic cells)/total cells.

RNA immunoprecipitation (RIP) assay

RIP assay was carried out following the procedures described in RIP kit (Millipore, Bedford, MA, USA). CNE2 cells were resuspended in complete RIP lysis buffer and incubated on ice. The magnetic beads were resuspended and rinsed with RIP wash buffer. Resuspended in 100 μL RIP wash buffer, the magnetic beads were incubated with 5 μg corresponding antibodies anti-SIRT1 and immunoglobulin G (IgG), centrifuged to remove the supernatant, supplemented with RIP wash buffer (0.5 mL) and isolated by a magnetic separator. Then, the sample was added with 900 μL RIP buffer, the cell RIP lysate was centrifuged at 14,000 rpm and resuspended by RIP wash buffer. Then, the supernatant (100 μL) was added to RIP reaction buffer containing the magnetic bead-antibody complex to 1 mL, labeled as input. Then, the mixture was centrifuged and separated by a magnetic separator. Supplemented with 0.5 mL RIP elution buffer in each tube, the magnetic bead-antibody complex was suspended and incubated with 150 μL proteinase K buffer to detach the antibody from the magnetic bead, which was followed by centrifugation and magnetic separation. RNA purification was performed on the obtained supernatant and RT-qPCR was applied to test gene expression.

Chromatin immunoprecipitation (ChIP) assay

Human SIRT1 and SIRT1-HY cDNA were inserted into retrovirus vector pMFG-puro. Retroviruses were generated by transiently transfection of pMFG-puro, MFG-SIRT1 and MFG-SIRT1-HY (deacetylase mutation) into H29D package cells. CNE2 cells were infected with retrovirus containing 8 g/mL polypropylene for 4 h. At 2 h post infection, CNE2 cells were treated with 2 g/mL puromycin (BD Biosciences, Palo Alto, CA, USA). The cells were lysed in a TNN buffer (120 mM NaCl, 40 mM Tris-HCl, pH 8.0, 0.5% NP-40, 1 mM phenylmethylsulphonyl fluoride, 1 mM sodium orthovanadate, 100 mM sodium fluoride and 1 μg/mL each of leupeptin, aprotinin and pepstatin). The obtained immunoprecipitates were heated with sodium dodecyl sulfate (SDS)-sample buffer and transferred onto 7.5% SDS-polyacrylamide gels, which was followed by electrophoresis separation. Then, the protein was transferred to a PROTRAN

Nitrocellulose Transfer Membrane (Schleicher&Schuell, Dassel, Germany) and probed with horseradish peroxidase-conjugated donkey anti-rabit IgG or anti-goat IgG by Luminal Reagent (Santa Cruz, CA, USA). Consistent with the procedures of ChIP kit (Millipore), the binding relation of PANDAR and SIRT1 in CNE2 cells was investigated.

Fluorescent in situ hybridization (FISH) assay

Bioinformatics website (http://lncatlas.crg.eu/) had predicted the subcellular localization of PANDAR before nucleocytoplasmic separation assay performed on PARIS™ Kit (Ambion, Austin, Texas, USA). CNE2 and 5-8F cells were resuspended in pre-cooled cellfractionation buffer (500 μL) and centrifuged to separate the supernatant (cytoplasm) and pellet (nucleus). The supernatant was added with an equal volume of preheated 2 × Lysis/Binding Solution and ethanol, and transferred to a filter column. The column was rinsed repeatedly and RNA on the filter was centrifuged to obtain dissolved cytoplasm RNA. The nucleus pellet was processed as described above to collect dissolved nuclear RNA. The cytoplasm and nuclear RNA were subjected to reverse transcription of cDNA on a M-MLV kit (Sigma-Aldrich). RT-qPCR was indicated to test PANDAR expression in the nucleus and cytoplasm.

The subcellular localization of PANDAR was verified by FISH assay. Seeded at 3×10^4 cells/wells in a 24-well plate with slides, cells were fastened by 4% paraformaldehyde (100 μL) and added with 0.5% TritonX-100 (100 μL). A prehybridization solution hybridization (100 μL) was added into each well before hybridization. The lncRNA PANDAR FISH probe (RiboBio Co., Ltd., Guangdong, China) and the hybridization solution were diluted at 1:50, and 100 μL mixture was added to each well for hybridization overnight. On the next day, the preheated 4 × SSC, 2 × SSC, and 1 × SSC were adopted to rinse cells in succession. Then, the cells were reacted with 10 μL DAPI working solution in each well and mounted. Five fields of view were selected to observe and photograph cells under a fluorescence microscope (Olympus, Tokyo, Japan).

Reverse transcription quantitative polymerase chain reaction (RT-qPCR)

Trizol (Invitrogen) was adopted for RNA extraction from tissues and cells, which was qualified by ultraviolet analysis and formaldehyde denaturation electrophoresis. RNA (1 μg) reverse transcription was acted with AMV to produce complementary DNA. qPCR was conducted by SYBR GEMeen. PCR primers were constructed and synthesized by Genechem (Shanghai, China) (Table 1). Real-time fluorescence quantitative PCR instrument (ABI 7500, ABI, Foster City, CA, USA) was employed for detection. Manually selected threshold at the lowest point of the parallel rise of each logarithmic amplification curve was the Ct value (Threshold cycle). Glyceraldehyde-3-phosphate dehydrogenase and U6 were the internal controls. Data was evaluated by $2^{-\Delta\Delta Ct}$ method.

Table 1
Primer sequence

Gene	Primer sequences
PANDAR	Forward: 5’-CTGTTAAGGTGGTGGCATTG-3’
	Reverse: 5’-GGAGGCTCATACTGGCTGAT-3’
SIRT1	Forward: 5’-TGGCAAAGGAGCAGATTAGTAGG-3’
	Forward: 5’-CATGGTATGATGATGGGTAGACC-3’
Ki-67	Reverse: 5’-TTCACAAGGACAAGTCGCAGCAGCT-3’
	Reverse: 5’-CTGCCACAAGAACTAGAGGATAAGA-3’
U6	Forward: 5’-CTCGCTTCGGCAGCACA-3’
	Reverse: 5’-AACGCTTCACGAATTTGCGT-3’
GAPDH	Forward: 5’-TGGGTGTGAACCATGAGAAG-3’
	Reverse: 5’-GTGTCGCTGTTGAAGTCAGA-3’

Note: PANDAR, long non-coding RNA promoter of CDKN1A antisense DNA damage activated RNA; SIRT1, sirtuin 1; GAPDH, glyceraldehyde-3-phosphate dehydrogenase

Western blot assay

Tissue and cell proteins were extracted and determined for protein concentration by following the instructions of bicinchoninic acid kit (Wuhan Boster Biological Technology Co., LTD., Hubei, China). The extracted protein was boiled with loading buffer and loaded on wells at 30 μg. Then, the protein was separated by 10% polyacrylamide gel (Boster), followed by transferring onto a polyvinylidene fluoride membrane and blockade in 5% bovine serum albumin. Next, the protein membrane was probed with primary antibodies SIRT1 (ab110304, 1:1000, Abcam, MA, USA), Ku70 (MA5-13110, 1:200, Invitrogen), phosphorylated (p)-PI3K (4228, 1:100), p-Akt (4060, 1:1000, both from CST) and β-actin (sc-47778, 1:3000, Santa Cruz Biotechnology) and with the corresponding secondary antibody (MT-Bio, Shanghai, China) and developed by chemiluminescence reagent. β-actin was an internal control. Bio-rad Gel Doc EZ imager (Bio-rad, CA, USA) was utilized to view the bands. The target bands were analyzed with Image J software (National Institutes of Health, Bethesda, Maryland, USA).

Statistical analysis

SPSS 21.0 (IBM, NY, USA) statistical software was indicated to data analysis. The measurement data were presented as mean ± standard deviation. Levene test and Kolmogorov-Smirnov test were carried out. For data of normal distribution and in homogeneity of variance, t test was applied for discrepancies between two groups and one-way analysis of variance (ANOVA) for those among multiple groups,

followed by Tukey post-hoc test. *P* was a two-sided test and its value less than 0.05 represented statistically significance.

Results

PANDAR is overexpressed in NPC tissues and cells and connected with inferior prognosis

RT-qPCR tested PANDAR expression in NPC and normal nasopharyngeal mucosa tissues and the results highlighted that NPC tissues expressed PANDAR at a high level, and especially radioresistant NPC tissues presented a higher PANDAR level than radiosensitive tissues (both $P < 0.001$) (Fig. 1A).

NPC patients were distributed into low expression and high expression groups referring to PANDAR median expression. The ties between PANDAR and clinicopathological traits in NPC patients were evaluated with the findings suggesting that PANDAR was connected with N stage, TNM stage and LNM. PANDAR expression in NPC tissues increased with the advances of N stage and TNM stage and it higher in LNM tissues (all $P < 0.05$). No connections were witnessed in PANDAR expression with age, gender or pathological grade (all $P > 0.05$) (Table 2). During the 60-month follow-up, the inferior prognosis was observed in NPC patients with high PANDAR expression, revealing that overexpressed PANDAR was connected with unsatisfactory prognosis (Fig. 1B).

Table 2
Correlation of PANDAR expression and clinicopathological traits of NPC patients [n(%)]

Clinicopathological data	Cases	PANDAR expression		χ2	*P*
		High expression group (n = 54)	Low expression group (n = 35)		
Age (years)				0.146	0.701
< 60	41	24(58.5)	17(41.5)		
≥ 60	48	30(62.5)	18(37.5)		
Gender				0.727	0.394
Male	51	29(56.9)	22(43.1)		
Female	38	25(65.8)	13(34.2)		
N stage				7.059	0.008
N0 + N1	38	17(44.7)	21(55.3)		
N2 + N3	51	37(72.5)	14(27.5)		
Pathological grade				3.512	0.173
Squamous cell carcinoma	30	20(66.7)	10(33.3)		
Non-keratosis	33	23(69.7)	10(30.3)		
Undifferentiation	26	11(42.3)	15(57.7)		
Clinical stage				8.025	0.005
I + II	47	22(46.8)	25(53.2)		
III + IV	42	32(76.2)	10(23.8)		
Lymph node metastasis				5.484	0.019
No	61	32(52.5)	29(47.5)		
Yes	28	22(78.6)	6(21.4)		
Note: This table uses chi-square test.					

RT-qPCR also indicated that in 6-10B, CNE2, 5-8F, HONE1 and C666-1 cells, PANDAR expression was overexpressed relative to that in NP69 cells (all $P < 0.05$). Selection of CNE2 and 5-8F cells for subsequent experiments was based on their presentation of greatly overexpressed PANDAR (Fig. 1C).

Predicted by the bioinformatics website, it was investigated that PANDAR was expressed in the nucleus and cytoplasm of NPC cells (Fig. 1D). Analyzed by nucleocytoplasmic separation assay and further

verified by FISH assay, it was supportive that PANDAR was expressed in the nucleus and cytoplasm of CNE2 and 5-8F cells, and higher PANDAR expression showed up in the cytoplasm rather than the nucleus (all $P < 0.05$), suggesting that PANDAR mainly functioned in the cytoplasm in NPC (Fig. 1E,F).

PANDAR and SIRT1 are overexpressed in radioresistant CNE2-IR and 5-8F-IR cells

CNE2 and 5-8F cells were induced into radioresistant CNE2-IR and 5-8F-IR cells by gradient radiation. Colony formation tested the radiosensitivity of CNE2-IR, 5-8F-IR and parental cells. It was pointed out that cell survival fraction decreased with the increase of radiation dose and CNE2-IR and 5-8F-IR cell survival fractions were higher versus to parental cells (both $P < 0.05$) (Fig. 2A, B), indicating the successful induction of radioresistant CNE2-IR and 5-8F-IR cells.

RT-qPCR tested PANDAR and SIRT1 expression in CNE2, 5-8F, CNE2-IR and 5-8F-IR cells. It was exhibited that PANDAR and SIRT1 were overexpressed in radioresistant cells rather than parental cells (both $P < 0.05$) (Fig. 2C), which initially suggested the potential connection between PANDAR/SIRT1 with NPC radioresistance.

To further explore PANDAR/SIRT1-oriented mechanism in NPC radioresistance, CNE2-IR and 5-8F-IR cells were transfected with depleted PANDAR or SIRT1. Detected by RT-qPCR and Western blot, the transfected cells were characterized by reduced PANDAR, SIRT1 and Ku70 expression, implying the successful transfection of PANDAR or SIRT1 low expression vectors (Fig. 2D-F).

Interfering PANDAR or SIRT1 delays radioresistant NPC cell proliferation and promotes apoptosis

Tests of proliferation (CCK-8 assay), colony-forming capacity (colony formation assay), Ki-67 mRNA expression (RT-qPCR) and apoptosis (flow cytometry) of CNE2-IR and 5-8F-IR cells highlighted that silencing PANDAR or SIRT1 inhibited proliferation, colony-forming capacity and Ki-67 mRNA expression and promoted apoptosis rate (Fig. 3A-D), which suggested the suppressive effects of PANDAR or SIRT1 down-regulation on radioresistant NPC proliferation and apoptosis.

Up-regulating SIRT1 mitigates PANDAR down-regulation-induced impacts on radioresistant NPC cell proliferation and apoptosis

Determined by CCK-8, colony formation, together with flow cytometry, it was manifested that SIRT1 elevation negated depleted PANDAR-induced impairments in proliferation, colony-forming capacity, and Ki-67 mRNA expression, as well as enhancement in apoptosis of NPC radioresistant cells (Fig. 4A-D). It was confirmed that overexpressed SIRT1 offset the effects of depleted PANDAR on radioresistant NPC cell proliferation and apoptosis.

Depleted PANDAR or SIRT1 inhibits PI3K/Akt pathway in NPC cells

The status of PI3K/Akt pathway was determined by Western blot detecting p-PI3K and p-Akt. In radioresistant NPC cells, interference with PANDAR or SIRT1 could decrease p-PI3K and p-Akt expression, indicating that inhibiting PANDAR and SIRT1 could suppress the activation of PI3K/Akt pathway (Fig. 5A,B).

To further illustrate role of SIRT1, Ku70 and PI3K/Akt pathway in NPC, we used measured PANDAR, SIRT1, Ku70, p-PI3K, and p-Akt in radioresistant NPC cells after down-regulation of PANDAR and up-regulation of SIRT1. The results showed that up-regulating SIRT1 reversed the effects of down-regulated PANDAR on SIRT1, Ku70, p-PI3K, and p-Akt expression (Fig. 5C,D), indicating that SIRT1 could offset the effects of PANDAR on SIRT1, Ku70, and PI3K/Akt pathway in NPC cells.

PANDAR recruits SIRT1 to promote Ku70 deacetylation

RNA from CNE2 cells was collected by RIP assay. The protein and RNA were co-precipitated with SIRT1 antibody and PANDAR enrichment level was detected by RT-qPCR. It was manifested that PANDAR was highly enriched (Fig. 6A). ChIP assay confirmed that SIRT1 could bind to the Ku70 promoter region (Fig. 6B).

Then, the possible interaction between SIRT1 and Ku70 protein in CNE2 cell lysates was investigated. The cell lysate was subsequently immunoprecipitated with anti-SIRT1 antibody and the immune complex was analyzed by western blot with anti-Ku70 antibody. The immunoprecipitation of SIRT1 from CNE2 cell lysates that locally overexpressing SIRT1 co-immunoprecipitated Ku70 (Fig. 6C). Anit-Ku70 antibody was utilized to immunoprecipitate the lysate and analyzed by western blot with SIRT1 antibody (Fig. 6D). On the other hand, in the immunoprecipitation of IgG antibody, Ku70 or SIRT1 protein couldn't be detected. It was hinted that SIRT1 and Ku70 could interact *in vivo* and form a complex with each other.

SIRT1 could physically form a complex with Ku70 [20], and Ku70 in an acetylated protein library immunoprecipitated with anti-acetyl lysine antibodies indicated that Ku70 could be acetylated in CNE2 cells (Fig. 6E). Ectopic expression of SIRT1 reduced acetylated Ku70 protein co-immunoprecipitated with anti-acetyl lysine antibody (Fig. 6F). However, the introduction of dominant negative SIRT1, SIRT1-HY led to the recovery of acetylated Ku70 protein level, and western blot assay with Ku70 antibody showed no detectable changes in total Ku70 protein expression. Therefore, this experiment elucidated that SIRT1 could deacetylate Ku70 protein *in vivo* by physically forming a complex with each other.

Discussion

NPC radioresistance can process to residual or recurrent tumors, which is the predominant factor causing radiotherapy failure [21]. Owing to that, a detailed comprehension about NPC radioresistance is beneficial to delve out constructive agents for sensitizing NPC cells to radiation. This work was conducted with the

major result summarized as PANDAR recruiting SIRT1 to promote Ku70 deacetylation, thereafter to activate PI3K/Akt pathway in radioresistant NPC.

To begin with, PANDAR expression was disclosed to up-regulate in NPC tissues and radioresistant NPC tissues, which was tied up with the unexpected prognosis of NPC victims. Cell experiments have further confirmed the observed findings in tissues. Also, PANDAR depletion assay was implemented to decipher its performance in radioresistant NPC cell proliferation, apoptosis, SIRT1, Ku70 and PI3K/Akt pathway. The discoveries highlighted that silencing PANDAR suppressed radioresistant NPC cell proliferation, promoted apoptosis, decreased SIRT1 and Ku70 expression and inactivated PI3K/Akt pathway. Actually, little few researches have clearly elucidated the precise position of PANDAR in NPC radioresistance, but some similar studies are included in this part to illustrate the negative role of overexpressed PANDAR in malignancies. Explored by a meta-analysis, overexpressed PANDAR is connected with reduced overall survival in colorectal cancer and with invasion depth, tumor stage, lymph node metastasis and distant metastasis [22]. In addition, PANDAR expression is elevated in prostate cancer and the incremental PANDAR is evidenced to connect with disease-free survival [23]. Functionally, detected in breast cancer, PANDAR expression is elevated which is tied up with LNM and advanced clinical stage, and PANDAR silencing diminishes breast cancer cell proliferation and colony-forming properties [24]. Besides that, a prior study focusing on clear cell renal cell carcinoma presents that elevated PANDAR is connected with advanced TNM stage and PANDAR impairment accredits to suppressed cell proliferation and promoted apoptosis [25]. Supported by an observational experiment, PANDAR elevation is manifested in ovarian cancer, which can mediate chemoresistance in disease [26]. Whatever, these literature has further convinced the phenotype of PANDAR in cancers.

Next, it was discovered that SIRT1 expression was raised in NPC tissues and cells and PANDAR could recruit SIRT1. SIRT1 depletion assay found that SIRT1 knockdown worked out the same outcomes of PANDAR depletion on cells. In order to explain the combined interplay of PANDAR and SIRT1 in NPC radioresistance, radioresistant NPC cells were transfected with PANDAR low expression and SIRT1 overexpression vectors in succession. The results indicated that SIRT1 restoration mitigated PANDAR down-regulation-induced effects on radioresistant NPC cells, SIRT1 and Ku70 expression and PI3K/Akt pathway. Till now, SIRT1 recruitment by PANDAR has nearly not been reported, which requires further confirmation. Experimentally, it is stresses out that SIRT1 is elevated in colorectal cancer, whose degradation impedes colorectal cancer cell proliferation [27]. Moreover, the incremental SIRT1 is also recognized in non-small lung cell cancer, which reinforces cell aggressive behaviors [28]. Similar to our study, SIRT1 inhibition is indicated to accelerate cell apoptosis and improve radiosensitivity of glioma [29]. Supplementarily, the pro-radiosensitive effects of SIRT1 inhibition has been documented in breast cancer, and SIRT1 depletion can ruin cell viability and promote apoptosis [30]. As investigated, Ku70 is one of the targets which are modulated by SIRT1 through deacetylation [12]. Intriguingly, SIRT1 suppression is responsible for the increment Ku70 acetylation in myeloid leukemia [31].

Conclusion

To sum up, this work has revealed that PANDAR enhances NPC radioresistance through down-regulating SIRT1 and Ku70 and suppressing PI3K/Akt pathway activation. Having replenished the known mechanism of NPC radioresistance, this work recommends a potential therapy axis in promoting NPC radiosensitivity. At a certain level, this study is finite in NPC radioresistance exploration, which needs to be supplemented by much investigations.

Declarations

Ethics Approval

This study was reviewed and approved by the ethics committee of Hubei Cancer Hospital, Tongji Medical College, Huazhong University of Science and Technology. All patients have signed an informed consent.

Consent to Participate

Written informed consent was obtained from the parents

Conflict of interest

The authors have no conflicts of interest to declare that are relevant to the content of this article.

Acknowledgement

This study was supported by the National Science Foundation of China (grant no. 81760545 to SWL Grant No.81772499 to XJL) ,the 5th Wuhan Young and Middle-aged Backbone Talent of Medical Training Project 2017 (2017 No. 51 to SWL),and Guilin Scientific Research and Technology Development Project NO.2016012706-4 to XSH the 7th Wuhan Young and Middle-aged Backbone Talent of Medical Training Project 2019 (2019 No. 87 to GLP),;also supported by the Applied Basic Research Program of Wuhan Science and Technology Bureau (Grant No. 2020020601012250 to XJL), and Cancer Research Program of National Cancer Center (No.NCC201817B052 to XJL).

References

1. Yao H, et al. LncRNA MSC-AS1 aggravates nasopharyngeal carcinoma progression by targeting miR-524-5p/nuclear receptor subfamily 4 group A member 2 (NR4A2). Cancer Cell Int. 2020;20:138.
2. Wu C, et al., *Radiation-Induced DNMT3B Promotes Radioresistance in Nasopharyngeal Carcinoma through Methylation of p53 and p21.* Mol Ther Oncolytics, 2020. **17**: p. 306–319.
3. Zhan Y, Fan S. Multiple Mechanisms Involving in Radioresistance of Nasopharyngeal Carcinoma. J Cancer. 2020;11(14):4193–204.

4. Zhong Q, Chen Y, Chen Z. LncRNA MINCR regulates irradiation resistance in nasopharyngeal carcinoma cells via the microRNA-223/ZEB1 axis. Cell Cycle. 2020;19(1):53–66.
5. He Y, et al. Long non-coding RNA PVT1 predicts poor prognosis and induces radioresistance by regulating DNA repair and cell apoptosis in nasopharyngeal carcinoma. Cell Death Dis. 2018;9(2):235.
6. Hu X, Jiang H, Jiang X. Downregulation of lncRNA ANRIL inhibits proliferation, induces apoptosis, and enhances radiosensitivity in nasopharyngeal carcinoma cells through regulating miR-125a. Cancer Biol Ther. 2017;18(5):331–8.
7. Sang Y, et al. LncRNA PANDAR regulates the G1/S transition of breast cancer cells by suppressing p16(INK4A) expression. Sci Rep. 2016;6:22366.
8. Siddique H, et al. Long Noncoding RNAs as Prognostic Markers for Colorectal Cancer in Saudi Patients. Genet Test Mol Biomarkers. 2019;23(8):509–14.
9. Yang Z, et al. Plasma long noncoding RNAs PANDAR, FOXD2-AS1, and SMARCC2 as potential novel diagnostic biomarkers for gastric cancer. Cancer Manag Res. 2019;11:6175–84.
10. Zheng GD, et al. Nobiletin induces growth inhibition and apoptosis in human nasopharyngeal carcinoma C666-1 cells through regulating PARP-2/SIRT1/AMPK signaling pathway. Food Sci Nutr. 2019;7(3):1104–12.
11. Maiese K. Moving to the Rhythm with Clock (Circadian) Genes, Autophagy, mTOR, and SIRT1 in Degenerative Disease and Cancer. Curr Neurovasc Res. 2017;14(3):299–304.
12. Fujita Y, Yamashita T. Sirtuins in Neuroendocrine Regulation and Neurological Diseases. Front Neurosci. 2018;12:778.
13. Yu D, et al. Silver nanoparticles coupled to antiEGFR antibodies sensitize nasopharyngeal carcinoma cells to irradiation. Mol Med Rep. 2017;16(6):9005–10.
14. Li J, et al. Niclosamide sensitizes nasopharyngeal carcinoma to radiation by downregulating Ku70/80 expression. J Cancer. 2018;9(4):736–44.
15. Zhang J, Zhou J, Xiao S. Shikonin inhibits growth, invasion and glycolysis of nasopharyngeal carcinoma cells through inactivating the phosphatidylinositol 3 kinase/AKT signal pathway. Anticancer Drugs; 2020.
16. Chen J, et al. CHL1 suppresses tumor growth and metastasis in nasopharyngeal carcinoma by repressing PI3K/AKT signaling pathway via interaction with Integrin beta1 and Merlin. Int J Biol Sci. 2019;15(9):1802–15.
17. Pan J, et al. A comparison between the Chinese 2008 and the 7th edition AJCC staging systems for nasopharyngeal carcinoma. Am J Clin Oncol. 2015;38(2):189–96.
18. Qu JQ, et al. MiRNA-203 Reduces Nasopharyngeal Carcinoma Radioresistance by Targeting IL8/AKT Signaling. Mol Cancer Ther. 2015;14(11):2653–64.
19. Zhang B, et al. Identification of heat shock protein 27 as a radioresistance-related protein in nasopharyngeal carcinoma cells. J Cancer Res Clin Oncol. 2012;138(12):2117–25.

20. Jeong J, et al. SIRT1 promotes DNA repair activity and deacetylation of Ku70. Exp Mol Med. 2007;39(1):8–13.
21. Chen Q, et al. ANXA6 Contributes to Radioresistance by Promoting Autophagy via Inhibiting the PI3K/AKT/mTOR Signaling Pathway in Nasopharyngeal Carcinoma. Front Cell Dev Biol. 2020;8:232.
22. Han L, et al. Prognostic and Clinicopathological Significance of Long Non-coding RNA PANDAR Expression in Cancer Patients: A Meta-Analysis. Front Oncol. 2019;9:1337.
23. Yang J, Zhao S, Li B. Long noncoding RNA PANDAR promotes progression and predicts poor prognosis via upregulating ROCK1 in prostate cancer. Eur Rev Med Pharmacol Sci. 2019;23(11):4706–12.
24. Li Y, Su X, Pan H. Inhibition of lncRNA PANDAR reduces cell proliferation, cell invasion and suppresses EMT pathway in breast cancer. Cancer Biomark. 2019;25(2):185–92.
25. Xu Y, et al. An increase in long non-coding RNA PANDAR is associated with poor prognosis in clear cell renal cell carcinoma. BMC Cancer. 2017;17(1):373.
26. Wang H, et al. The cisplatin-induced lncRNA PANDAR dictates the chemoresistance of ovarian cancer via regulating SFRS2-mediated p53 phosphorylation. Cell Death Dis. 2018;9(11):1103.
27. Yu L, et al. Ubiquitination-mediated degradation of SIRT1 by SMURF2 suppresses CRC cell proliferation and tumorigenesis. Oncogene. 2020;39(22):4450–64.
28. Jiang W, et al. Hsa-miR-217 Inhibits the Proliferation, Migration and Invasion in Non-small-cell Lung Cancer Cells Via Targeting SIRT1 and p53/KAI1 Signaling. Balkan Med J; 2020.
29. Li T, et al. MicroRNA-320 Enhances Radiosensitivity of Glioma Through Down-Regulation of Sirtuin Type 1 by Directly Targeting Forkhead Box Protein M1. Transl Oncol. 2018;11(2):205–12.
30. Zhang X, et al. miR-22 suppresses tumorigenesis and improves radiosensitivity of breast cancer cells by targeting Sirt1. Biol Res. 2017;50(1):27.
31. Zhang W, et al. SIRT1 inhibition impairs non-homologous end joining DNA damage repair by increasing Ku70 acetylation in chronic myeloid leukemia cells. Oncotarget. 2016;7(12):13538–50.

Figures

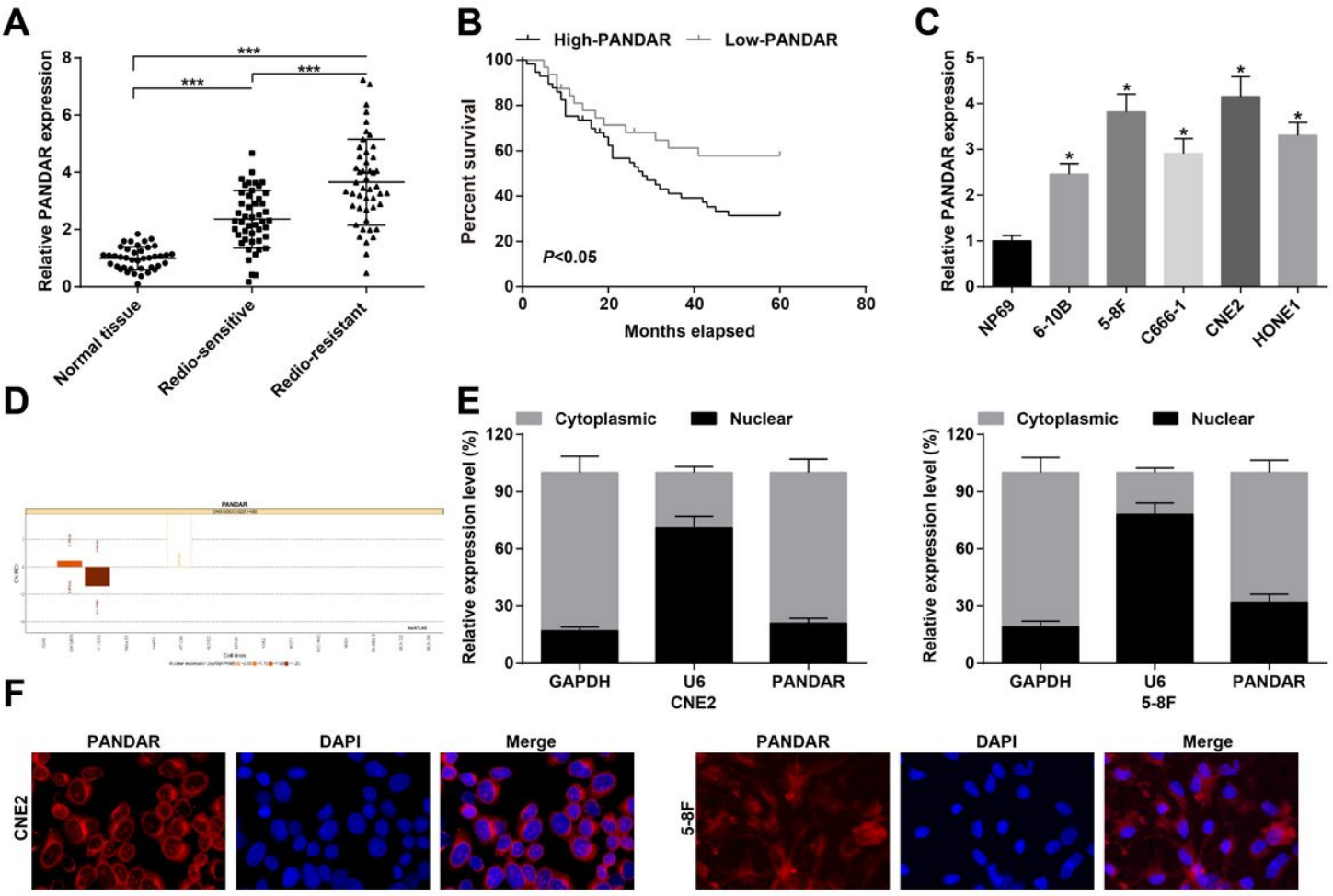

Figure 1

PANDAR is overexpressed in NPC and connected with inferior prognosis. A. RT-qPCR to detect PANDAR expression in tissues; B. NPC patient survival with high and low PANDAR expression levels; C. RT-qPCR to detect PANDAR expression in NPC cells and normal cells; D. Bioinformatics website to predict PANDAR localization; E. Nucleocytoplasmic separation assay to detect PANDAR localization; F. FISH assay to verify PANDAR localization; Repetitions = 3. t test was applied for discrepancies between two groups and one-way ANOVA for those among multiple groups, followed by Tukey post-hoc test. In Figure B, Kaplan-Meier analysis was applied; * P < 0.05 compared with NP69 cells; *** represented P < 0.001.

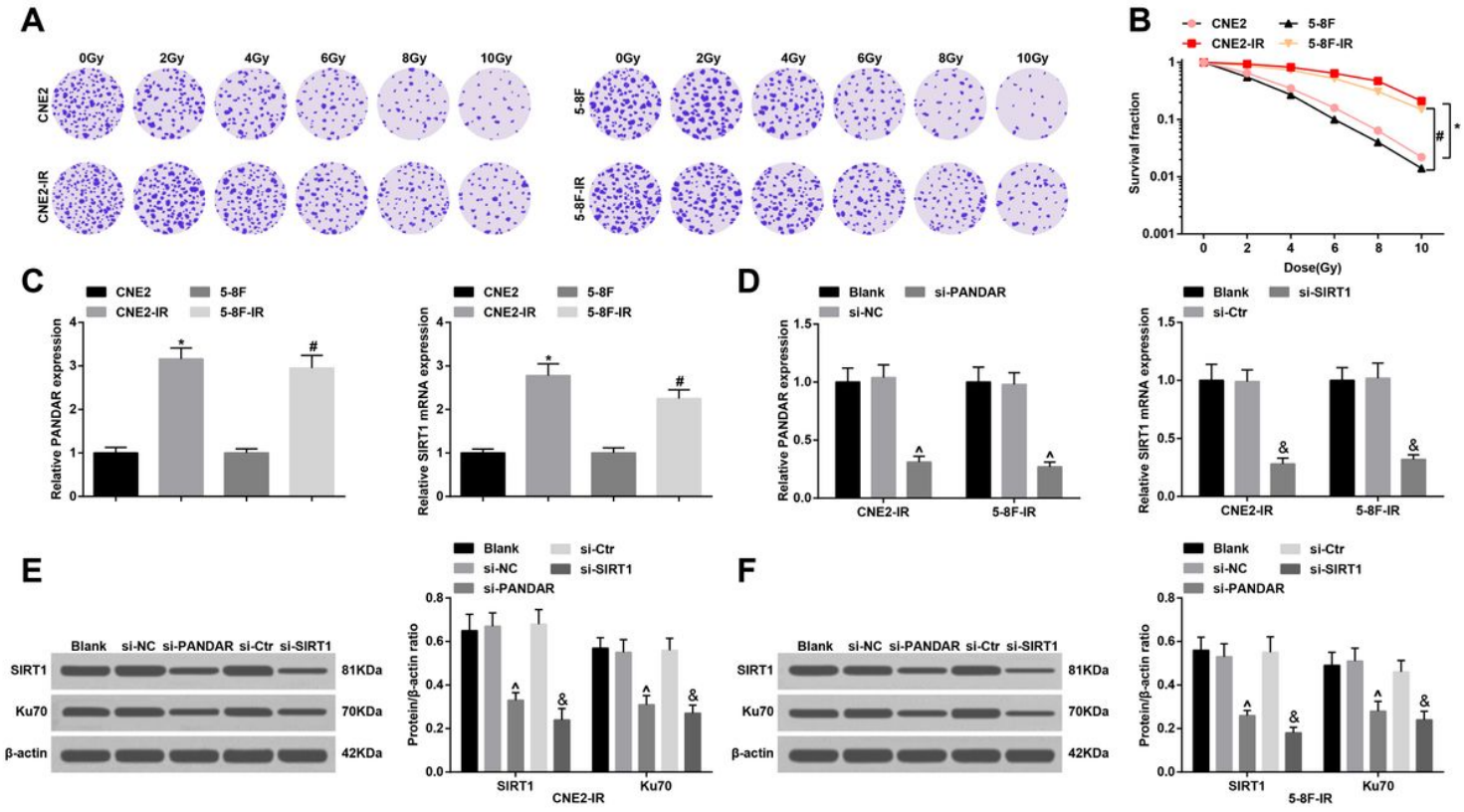

Figure 2

PANDAR and SIRT1 are overexpressed in radioresistant CNE2-IR and 5-8F-IR cells. A. The effect of different ionizing radiation on the number of colonies on CNE2-IR, 5-8F-IR and parental cells; B. CNE2-IR, 5-8F-IR and parental cell radiotherapy sensitivity; C. RT-qPCR to detect PANDAR and SIRT1 expression levels in CNE2-IR, 5-8F-IR and parental cells; D. RT-qPCR to detect PANDAR and SIRT1 expression levels in CNE2-IR and 5-8F-IR cells after interference with PANDAR or SIRT1; E. Western blot to detect the protein expression levels of SIRT1 and Ku70 in CNE2-IR cells after interference with PANDAR or SIRT1; F. Western blot to detect the protein expression levels of SIRT1 and Ku70 in 5-8F-IR cells after interference with PANDAR or SIRT1; Repetitions = 3. One-way ANOVA was performed for discrepancy among multiple groups, followed by Tukey post-hoc test; * $P < 0.05$ compared with CEN2 cells; # $P < 0.05$ compared with 5-8F cells; ^ $P < 0.05$ compared with the si-NC group; & $P < 0.05$ compared with the si-Ctr group.

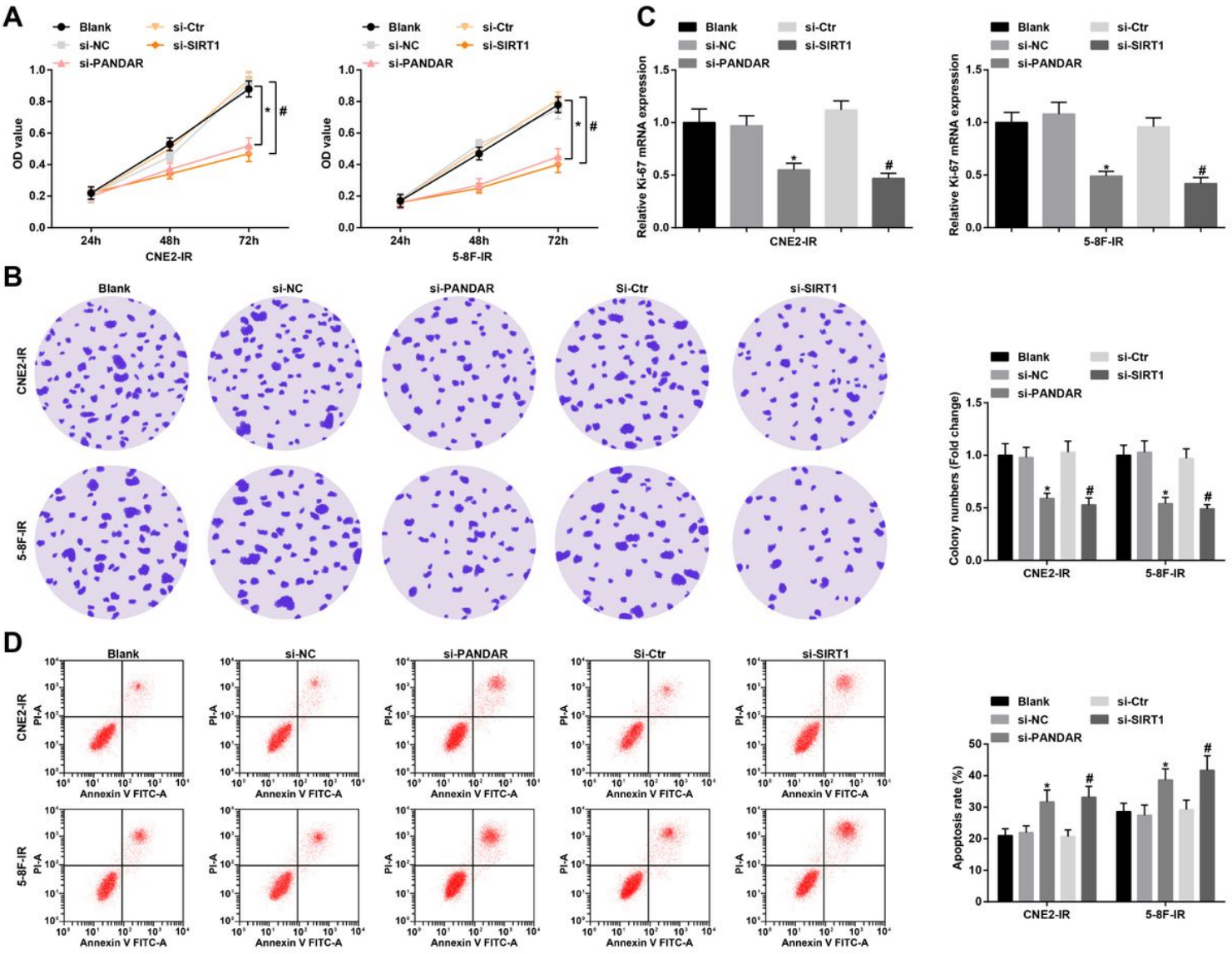

Figure 3

Interfering PANDAR or SIRT1 delays radioresistant NPC cell proliferation and promotes apoptosis. A. CCK-8 assay to detect CNE2-IR and 5-8F-IR cell proliferation; B. Colony formation assay to detect colony number of CNE2-IR and 5-8F-IR cells; C. RT-qPCR to detect Ki-67 mRNA expression in CNE2-IR and 5-8F-IR cells; D. Flow cytometry to detect CNE2-IR and 5-8F-IR cell apoptosis; Repetitions = 3. One-way ANOVA was performed for discrepancy among multiple groups, followed by Tukey post-hoc test; * $P < 0.05$ compared with the si-NC group; # $P < 0.05$ compared with the si-Ctr group.

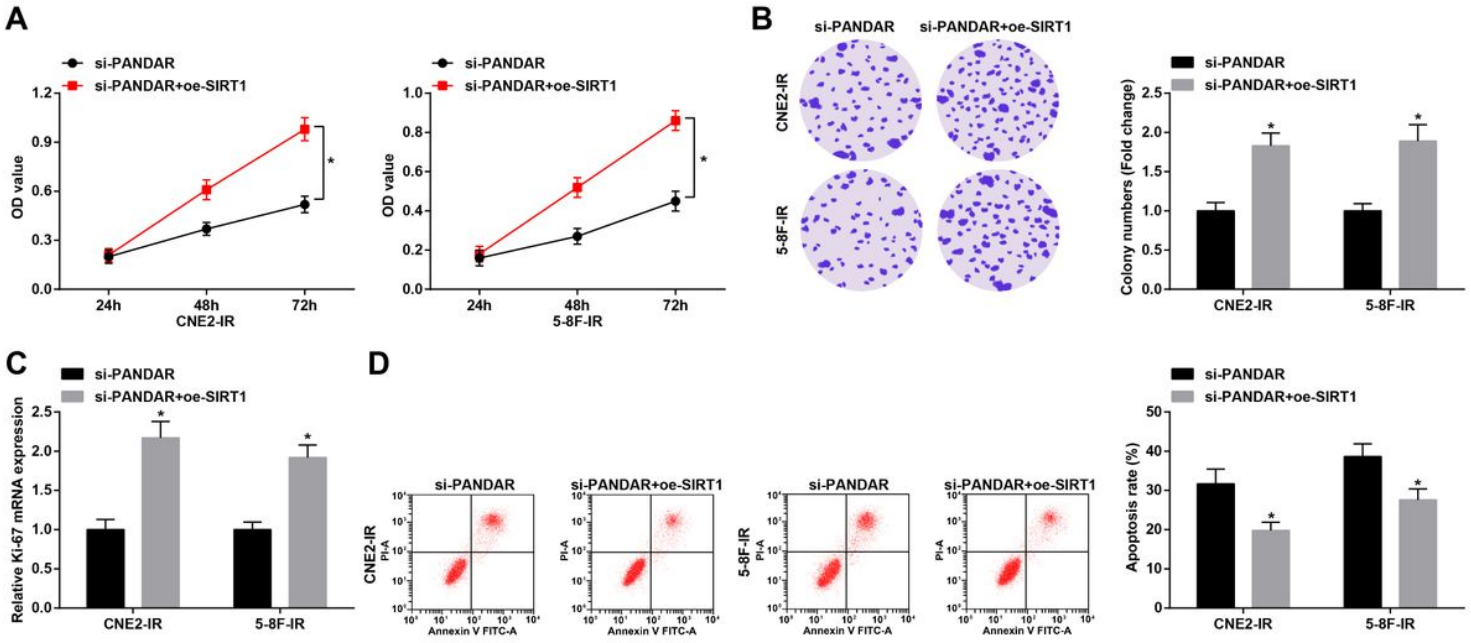

Figure 4

Up-regulating SIRT1 mitigates PANDAR down-regulation-induced impacts on radioresistant NPC cell proliferation and apoptosis. A. CCK-8 assay to detect CNE2-IR and 5-8F-IR cell proliferation; B. Colony formation assay to detect colony number of CNE2-IR and 5-8F-IR cells; C. RT-qPCR to detect Ki-67 mRNA expression in CNE2-IR and 5-8F-IR cells; D. Flow cytometry to detect apoptosis of CNE2-IR and 5-8F-IR cells; Repetitions = 3. t test was performed for discrepancy between two groups; * P < 0.05 compared with the si-PANDAR group.

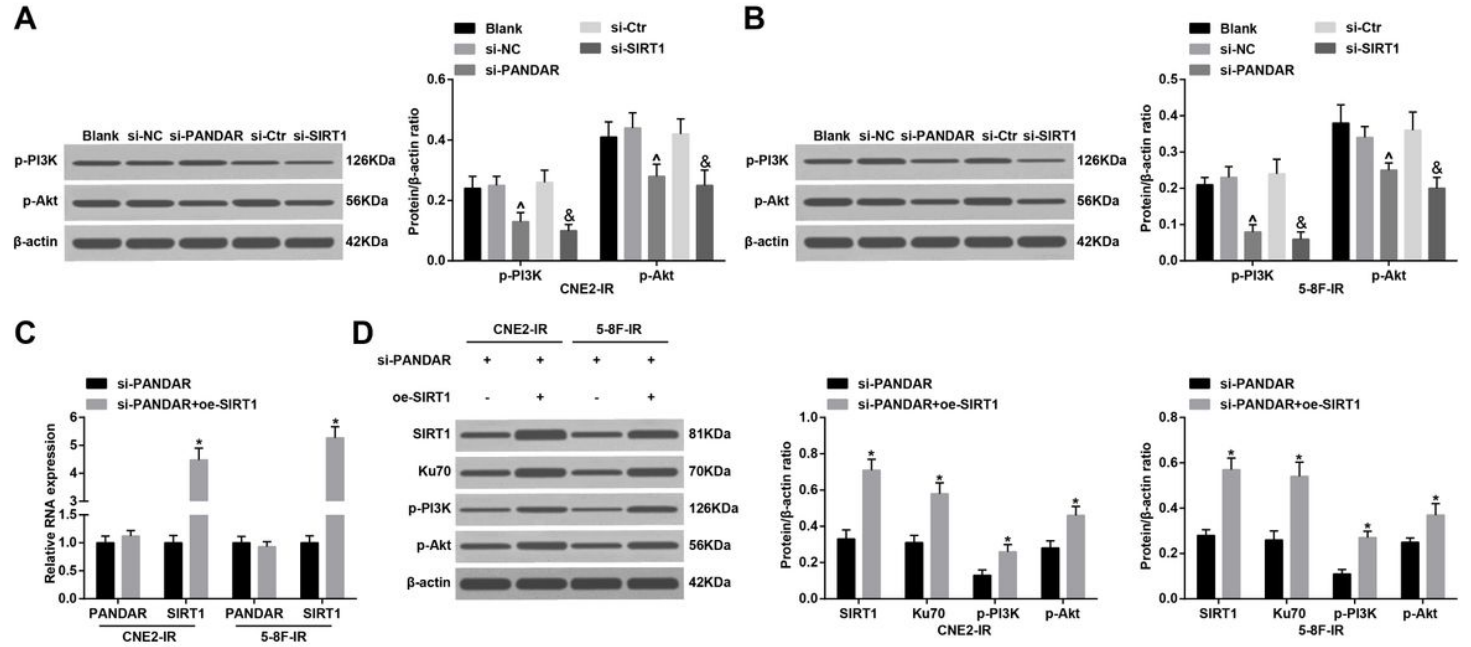

Figure 5

Depleted PANDAR or SIRT1 inhibits PI3K/Akt pathway in NPC cells. A/B. Western blot to detect p-PI3K and p-Akt protein expression after CNE2-IR and 5-8F-IR cells interfered with PANDAR or SIRT1; C. RT-qPCR to detect PANDAR and SIRT1 expression in CNE2-IR and 5-8F-IR cells after down-regulating PANDAR and up-regulating SIRT1; D. Western blot assay to detect SIRT1, Ku70 and p-PI3K and p-Akt protein expression in CNE2-IR and 5-8F-IR cells after down-regulating PANDAR and up-regulating SIRT1; Repetitions = 3. t test was performed for discrepancy between two groups; * compared with the si-PANDAR group.

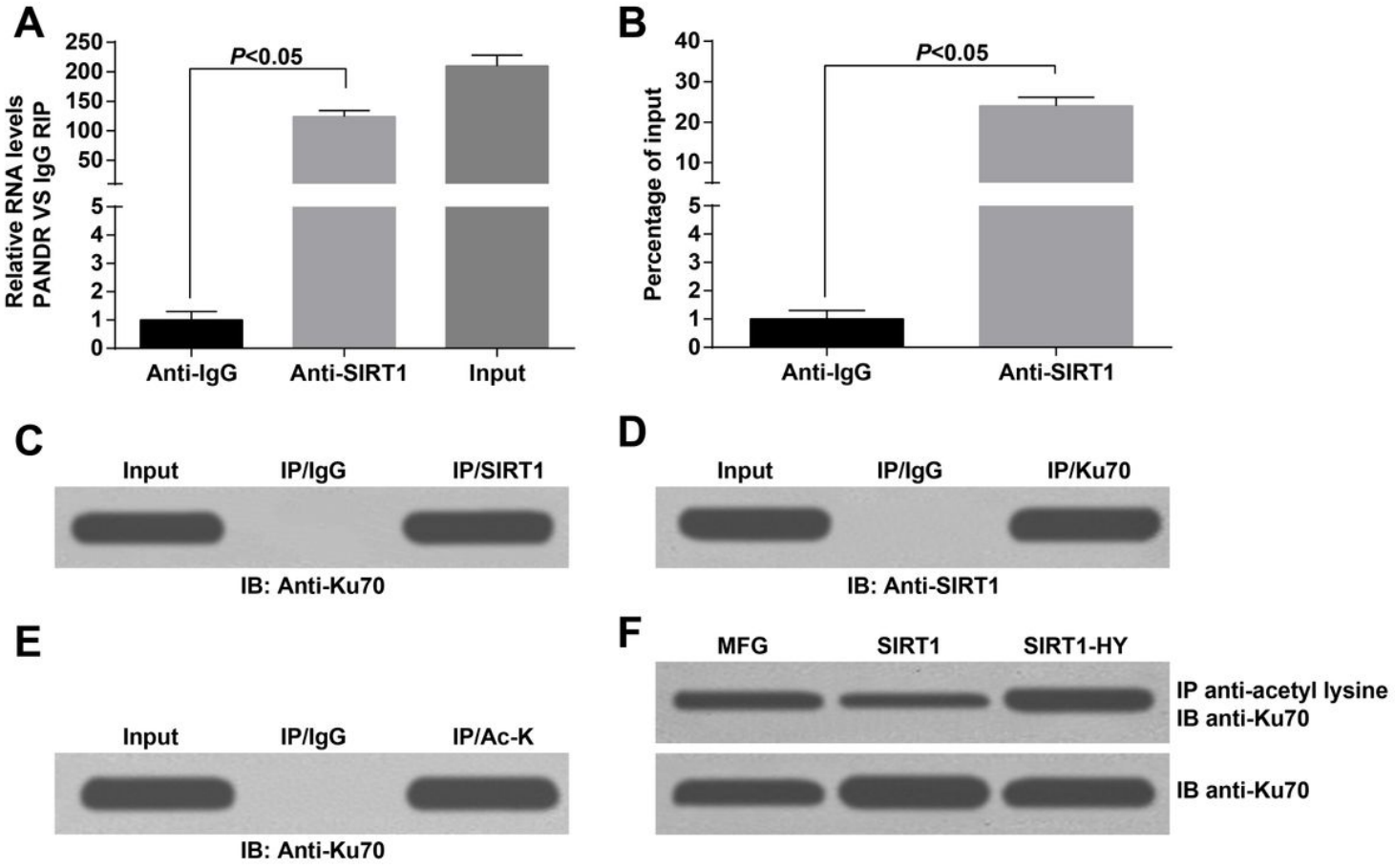

Figure 6

PANDAR recruits SIRT1 to promote Ku70 deacetylation. A. RNA immunoprecipitation was extracted from the anti-SIRT1, IgG or 10% input in CNE2 cells, and RNA expression was detected by RT-qPCR in the immunoprecipitation (SIRT1 enriched PANDAR was expressed by the multiple of IgG enriched PANDAR); B. Chip-RT-qPCR assay detected SIRT1 binding abundance of Ku70 promoter region in CNE2 cells, IgG was a NC; C&D. Cell lysates were immunoprecipitated with anti-SIRT1 (C), anti-Ku70 antibody (D) or IgG antibody, and probed with each other by anti-Ku70 (C) or anti-SIRT1 antibody (D) respectively; E. The cell lysates were immunoprecipitated with antibody against acetylated-lysine and probed with anti-Ku70 antibody; F. Cell lysates were immunoprecipitated with anti-acetylated lysine (above) or anti-Ku70 antibody (below), and then western blot was performed to detect Ku70 protein.